ADVANCES IN ATMOSPHERIC SCIENCES, VOL. 32, JUNE 2015, 807–820

A Diagnostic Analysis on the Effect of the Residual Layer in Convective Boundary Layer Development near Mongolia Using 20th Century Reanalysis Data

HAN Bo*, ZHAO Cailing, LÜ Shihua, and WANG Xin

Key Laboratory of Land Surface Process and Climate Change in Cold and Arid Regions, Cold and Arid Regions Environmental and Engineering Research Institute, Chinese Academy of Sciences, Lanzhou 730000

(Received 23 July 2014; revised 29 September 2014; accepted 29 October 2014)

ABSTRACT

Although the residual layer has already been noted in the classical diurnal cycle of the atmospheric boundary layer, its effect on the development of the convective boundary layer has not been well studied. In this study, based on 3-hourly 20th century reanalysis data, the residual layer is considered as a common layer capping the convective boundary layer. It is identified daily by investigating the development of the convective boundary layer. The region of interest is bounded by (30°–60°N, 80°–120°E), where a residual layer deeper than 2000 m has been reported using radiosondes. The lapse rate and wind shear within the residual layer are compared with the surface sensible heat flux by investigating their climatological means, interannual variations and daily variations. The lapse rate of the residual layer and the convective boundary layer depth correspond well in their seasonal variations and climatological mean patterns. On the interannual scale, the correlation coefficient between their regional averaged (40°–50°N, 90°–110°E) variations is higher than that between the surface sensible heat flux and convective boundary layer depth. On the daily scale, the correlation between the lapse rate and the convective boundary layer depth in most months is still statistically significant during 1970–2012. Therefore, we suggest that the existence of a deep neutral residual layer is crucial to the formation of a deep convective boundary layer near the Mongolian regions.

Key words: convective boundary layer, residual layer, lapse rate, surface sensible heat flux, wind shear

Citation: Han, B., C. L. Zhao, S. H. Lü, and X. Wang, 2015: A diagnostic analysis on the effect of the residual layer in convective boundary layer development near Mongolia using 20th century reanalysis data. *Adv. Atmos. Sci.*, **32**(6), 807–820, doi: 10.1007/s00376-014-4164-6.

1. Introduction

The convective boundary layer (CBL) is the main manifestation of the atmospheric boundary layer (ABL) during the daytime (Stull, 1988; Garratt, 1994; Zilitinkevich, 2012). Its development and maintenance have a direct influence on many atmospheric phenomena, such as cloud formation (Barthlott et al., 2010; Thornton et al., 2011) and pollutant distribution (Lin and McElroy, 2010; Banta et al., 2011). Therefore, the factors that affect the growth of the CBL have been discussed for many years (Stull, 1988; Garratt, 1994; Moeng and Sullivan, 1994; Bianco et al., 2011; Maronga and Raasch, 2013).

The buoyancy caused by the underlying heating is often suggested to be the most important factor (Moeng and Sullivan, 1994; Maronga and Raasch, 2013), which is easily accepted because it exhibits a similar diurnal and annual variation as the CBL depth, especially over continents. Furthermore, its global spatial distribution supports this theory because a deep CBL is often reported over arid or semi-arid regions. The dominance of the surface sensible heat flux on the CBL has also been confirmed by using numerical simulation results (such as large eddy models). However, other factors such as the heterogeneity scale and the coherent structure of turbulence can also significantly impact the local CBL development (Avissar and Schmidt, 1998; Roy and Avissar, 2000; Maronga and Raasch, 2013).

Many factors can influence the depth of a CBL (Pan and Mahrt, 1987; Bianco et al., 2011). Most of these factors affect the atmospheric thermal or dynamic processes near the land surface (i.e. by changing the energy source of the thermals within the CBL) (Lenschow and Stephens, 1980). The thermals within the CBL will continue to rise until reaching the inversion layer (or entrainment zone), when their kinetic energy in the vertical direction is totally consumed. Because

* Corresponding author: HAN Bo
Email: hanbo@lzb.ac.cn

the entrainment process raises the top of the CBL, the thermal structure within the inversion layer can affect the CBL evolution by modifying the entrainment rate (Gentine et al., 2013b; Gentine et al., 2013a). However, such an impact may be no less important than that of the surface sensible flux because some early studies just define the inversion layer as a 0-order jump of potential temperature and the mixed layer top buoyancy flux is a constant fraction of the surface buoyancy flux (Tennekes, 1973; Garratt, 1994). Moeng and Sullivan (1994) compared the development of a shear-driven and buoyancy-driven planetary boundary layer (PBL) in a large eddy model; the effect of surface heating overwhelmed that of wind shear. However, because the actual atmosphere is more complicated than that in an idealized numerical simulation, the potential contributions of other factors on CBL development need to be reinvestigated.

The atmospheric layer above the inversion layer is usually called the free atmosphere layer, within which the turbulent movement can be neglected. When the stratification of the lower free atmosphere layer is neutral, it can be referred to as a residual layer because its characteristics (mean state and concentration variables) are generally observed to be initially the same as those of the recently decayed mixed layer (Stull, 1988; Marsham et al., 2008; Huang et al., 2010; Freire and Dias, 2013). In this type of CBL, when the potential temperature in the mixed layer approaches the value in the residual layer, the inversion layer disappears and the thermals in the mixed layer move freely upward into the residual layer. Some of the literature refers to such a process as a coupling between the residual layer and CBL (Stensrud, 1993; Fochesatto et al., 2001). Related works can be traced back to Stull (1976) and his classic schematic figure for the planetary boundary layer cycle (Stull, 1988).

In recent decades, a stable residual layer capping the CBL over the Sahara region (i.e. Sahara residual layer) has been reported via coordinated research flights over the Saharan heat low (Parker et al., 2005; Marsham et al., 2008; Messager et al., 2010). These studies are more concerned with the effect of the residual layer on dust transport; the effect of such a large-scale residual layer on the local CBL development has not been well studied. Recently, Han et al. (2012) reported that when a neutral residual layer caps the CBL, the growth of the CBL will be mainly determined by the lapse rate of the residual layer rather than by the intensity of the surface heat flux. However, their results are not conclusive because the number of observation cases used was rather small. Generally speaking, although the existence and the potential impact of the residual layer on the CBL development have been mentioned, these results have not been verified in long-term studies or over widespread regions.

In this study, we focus mainly on the CBL development over the region of (40°–50°N, 90°–110°E) near Mongolia (30°–60°N, 70°–130°E), where most of the arid and semi-arid regions of East Asia are located. We choose this region mainly because of its deep CBL during the summer, but also because a deep and neutral residual layer has been observed at (39°28′N, 102°22′E). The reanalysis data used and our definition of the residual layer for the reanalysis data are introduced in section 2. The climatological mean features of the residual layer and their co-variations with the CBL at different time scales are presented in section 3. The major conclusions and a discussion are provided in section 4.

2. Data and method

2.1. *The reanalysis data*

By using radiosondes in field observation experiments, the detailed vertical profile of atmospheric variables can be obtained. The top of the CBL is usually identified from a jump of (virtual) potential temperature or the mass ratio of water vapor. However, such types of observation data are temporally and spatially limited. For example, global radiosonde data, such as the Integrated Global Radiosonde Archive (Elliott and Gaffen, 1991; Durre et al., 2006), may have a coarse resolution in the vertical direction and vary among sites; thus, these datasets are not suitable for CBL research. Therefore, the datasets used in this study should present a continuous CBL depth over a long period and cover a wide region. Considering these criteria, we choose the 20th century reanalysis (20R) dataset. Its atmospheric boundary layer depth (and other variables in the surface layer) is provided every 3 hours, which is comparable to the time interval of a radiosonde observation. The variables on multi-pressure levels in 20R are produced every 6 hours. Details of the 20R dataset can be referred to in the works of Compo et al. (2011) and Saha et al. (2010).

The depth of an ABL (h hereafter) from 20R is calculated following the non-local PBL diffusion scheme (Troen and Mahrt, 1986; Holtslag et al., 1990; Holtslag and Boville, 1993; Hong and Pan, 1996):

$$h = \frac{Ri_{\mathrm{bc}}\theta_{\mathrm{va}}|U(h)|^2}{g[\theta_{\mathrm{v}}(h) - \theta_{\mathrm{s}}]}\,, \tag{1}$$

where Ri_{bc} is the critical bulk Richardson number, $U(h)$ and $\theta_{\mathrm{v}}(h)$ are the horizontal wind speed and virtual potential temperature at the top of the ABL, respectively, and θ_{va} is the virtual potential temperature at the lowest level of the model. θ_{s} is the appropriate temperature near the surface:

$$\theta_{\mathrm{s}} = \theta_{\mathrm{va}} + b\frac{\overline{(w'\theta'_{\mathrm{v}})_0}}{\boldsymbol{u}^*\phi_{\mathrm{m}}h}\,, \tag{2}$$

where

$$\phi_{\mathrm{m}} = \left(1 - 1.6\frac{h}{L}\right)^{-0.25}\,, \tag{3}$$

b is an experimental constant, $\overline{(w'\theta'_{\mathrm{v}})_0}$ is the virtual heat flux at the surface, $\boldsymbol{u}^*$ is the friction velocity, and L is the Monin–Obukhov length scale. Equation (3) is suitable only for neutral or unstable conditions $[\overline{(w'\theta'_{\mathrm{v}})_0} \leqslant 0]$, which is a condition for the formation of the CBL. The details and parameters used in the calculation of h in 20R are provided by Hong and Pan (1996).

A clear relationship between h and other variables cannot easily be identified from Eqs. (1) to (3), but it is clear that h is determined mainly by three factors: the sensible heat flux at the surface, the vertical shear of horizontal wind speed and the profile of the virtual potential temperature. Therefore, if 20R can generally describe the 3D thermodynamic structure of the atmosphere and the surface turbulent heat fluxes in the study region, then the depth of the ABL should be close to reality, and the potential cause of the variation of h can be discussed by using statistical analysis. However, it is important to remember that the reanalysis data are based on a combination of real observations and model results, so the uncertainty of the ABL depth given by 20R should not be neglected. Here, we compare the observed ABL depths in Badain Jaran desert (39°28′N, 102°22′E) during 3–7 July 2012 with that given by 20R (Fig. 1). Clear differences can be found. However, it should be noted that moments of observation and reanalysis are not identical. Even so, the 20R gives a shallow CBL on 6 July and deep ones on 4 and 5 July. Moreover, the potential temperature profiles also show similar features with observations. A long-term intercomparison of ABL depth between observation and reanalysis is difficult to apply because the observation data are short and limited. If the surface turbulent heat fluxes, 3D atmospheric fields and the depth of the ABL given by 20R are reasonable, then it can be used to discuss the importance of the residual layer for the CBL development.

The area of interest in this study is the arid and semi-arid regions near Mongolia, over which distinguishable depth differences exist between a nocturnal boundary layer and the CBL, and a deep and neutral residual layer has been monitored using radiosondes (Han et al., 2012). The daily maximum ABL layer ($h_{\max}$), which primarily represents the final status of the CBL development, is the focus of this study. As such, defining the residual layer is the most crucial step and will be given next.

2.2. *Identifying the residual layer in reanalysis data*

Because a near-neutral layer above the CBL has been suggested to be referred to as the residual layer in previous works, e.g. Stull (1988) and Freire and Dias (2013), the name of the residual layer will also be used in this study. It should be noted that, based on many observational studies, a (neutrally stratified) residual layer capping the CBL is not always apparent, which makes discussion of the connection between a residual layer and the CBL difficult. Therefore, the residual layer considered in this study does not need to be neutral; instead, it is considered as a common layer above the CBL with its characteristics varying with time. In other words, the residual layer represents the upper external environment that can significantly affect the local CBL development in this study.

The classical theory for the diurnal cycle of the ABL suggests that a residual layer should cap the CBL at the early stage of the CBL's development (Stull, 1988). However, because thermodynamic processes due to atmospheric advection or radiation transmission can alter the stratification status in the mid-layer of the atmosphere, a distinguishable neutrally stratified layer capping on the CBL is not always apparent. Thus, many studies considered the layer above the CBL as the free atmosphere layer rather than the residual layer (Fedorovich et al., 2004; Zilitinkevich et al., 2012). Recently, Freire and Dias (2013) suggested that when the lapse rate of the layer above the CBL is close to zero, then it should be called the residual layer; otherwise, it should be called the free atmosphere layer. Furthermore, they even suggested a two-residual layer structure exists above the CBL. This approach is valuable for site observations with dense vertical resolutions, but it is certainly not appropriate for reanalysis such as 20R, which has a vertical resolution of approximately 50 hPa (approximately 500 m).

Several studies based on observations report that the CBL top tends to jump when a deep and neutral stratified residual layer caps the CBL (Han et al., 2012; Freire and Dias, 2013). Although the ABL development is different between observation and 20R, both can reproduce the jump of the CBL top at least over Badain Jaran desert (39°28′N, 102°22′E), except for on 6 July 2012 (Fig. 1). Moreover, the maximum growth of the observed CBL depth is approximately equal to the depth of the near-neutral layer. The suppression of CBL development on 6 July is due to the precipitation over the observation site before noon. It should be noted that during summer, the cloud cover within the boundary layer is nearly 10% over the region concerned (figure omitted); therefore, the CBL there is mainly developed on a clear day. For other seasons, the cloud cover north of 50°N can be greater than 50%. Because the potential coupling between the residual layer and CBL is most significant in summer (sections 3.2 and 3.3), the cloud effect will not be considered in this study.

Based on the discussions above, the residual layer is defined in 20R as follows (Fig. 2):

(1) The layer capping the CBL is called the residual layer, regardless of the stratification status of the atmospheric column. Therefore, a stable stratified residual layer is allowed in this study. However, it should be noted that a residual layer must be eroded by a mixed layer on the day.

(2) The depth of the residual layer is equal to the fastest growth of the CBL for each 3-h period during the day. Its lower and upper boundaries (see Fig. 2) are defined as the height of the CBL before and after the CBL maximum growth, respectively.

(3) The features of a residual layer can be calculated by interpolating the pressure level variable to the location of the residual layer boundaries. The moments for the reanalysis data used to describe the residual layer should be in front of that when the CBL erodes into the residual layer (e.g. the residual layer on 5 July as in Fig. 2).

With these considerations, the residual layer is not only determined from the profile of the atmosphere but also from the feature of CBL development. An intercomparison of residual layer structure over the Badain Jaran desert (39°28′N, 102°22′E) between observation and reanalysis is given in Table 1. Although there are some differences, 20R generally captures the stratification variation within the

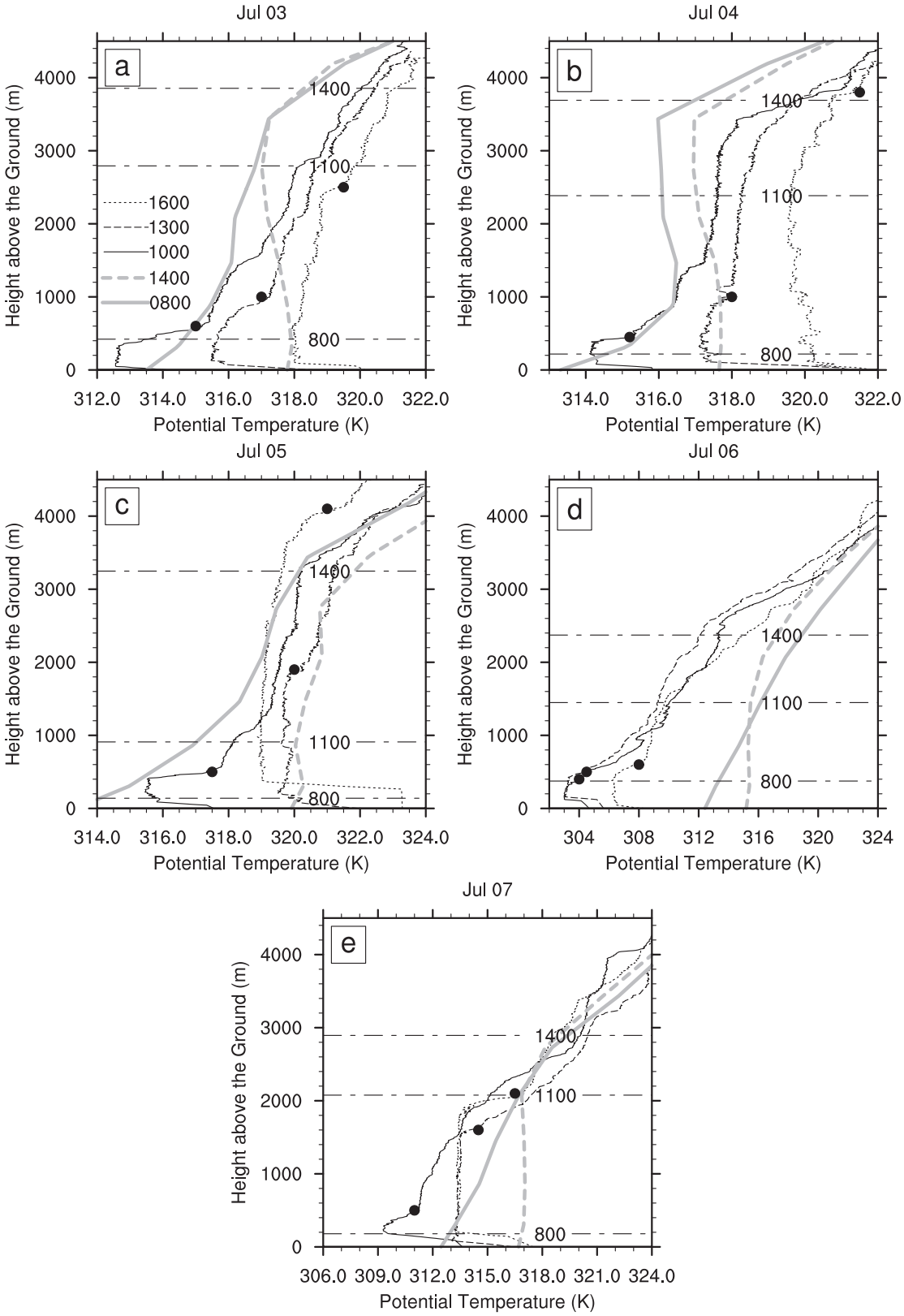

Fig. 1. Vertical profiles of potential temperature from 3 to 7 July (a–e) over Badain Jaran desert (39°28′N, 102°22′E) obtained using radiosondes (IMET-AB). The observations at three times, 1000 LST (solid line), 1300 LST (dashed line) and 1600 LST (dotted line) are given. The top of the CBL is indicated as filled black dots. The potential temperature profiles given by 20R (for the times of 0800 and 1400 LST) using linear interpolation are given as thick gray lines. The ABL heights given by 20R are given as short-dash–long-dash horizontal lines (for the times of 0800, 1100 and 1400 LST).

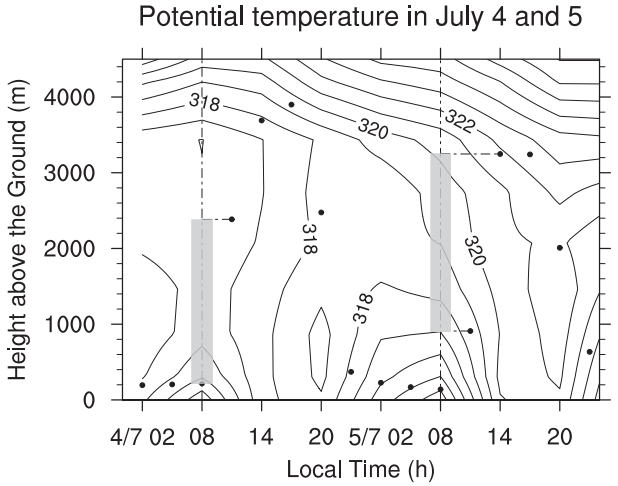

Fig. 2. An illustration to show how a local residual layer is defined using 20R. Black dots are 3-hourly boundary layer heights; contours show the variation of the potential temperature profile (intervals: 2 K). The results for the location (39°28′N, 102°22′E) from 4 to 5 Jul are shown. The residual layer defined in this study is indicated by gray boxes. Note that the time interval for potential temperature is 6 hours, while that for ABL height is 3 hours.

Table 1. An intercomparison of the lapse rate of the residual layer (γ_R, units: 10^{-3} K m^{-1}) between observation and reanalysis in 2012. Here, the reanalysis data have been linearly interpolated to the location of (39°28′N, 102°22′E). The observed lapse rate is derived from the profile at 1000 LST, while that from reanalysis is calculated using the method given in section 2.2 (Fig. 1).

	3 Jul	4 Jul	5 Jul	6 Jul	7 Jul
Observation	1.67	0.92	1.07	5.24	2.27
20R	1.12	0.77	1.36	3.11	1.84

residual layer during the observation period. The applicability of this definition over other regions can also be discussed if there are sufficient reliable observations. Following the residual layer definition above, the daily features of the residual layer can be obtained from 20R. The daily maximum ABL depth, which is highly correlated with the daytime mean depth of CBL, is used to represent the daily depth of the CBL. With these considerations, the connections between the residual layer and the CBL are of particular interest in this study.

Using reanalysis data with coarse vertical resolution to discuss the detailed structure of sub-layers within or near the ABL should always be caution. Here, the depth of the residual layer is usually greater than 1000 m over the region concerned (Fig. 3), which means there are at least two pressure levels involved in a residual layer for a general situation. If the stratification of the residual layer changes little in the vertical direction, the vertical resolution of 20R should be appropriate to describe the residual layer structure. By using this definition, the depth of the residual layer will be quite closely correlated with the CBL depth on the same day. However, the features of the defined residual layer, such as the lapse rate of the potential temperature (γ_R) and horizontal wind shear in the vertical direction (W_{sh}), are independent of the CBL structure and can represent the main upper environment of a developing CBL. Therefore, the residual layer we define here is the atmospheric layer that is most likely to be coupled with the CBL. This is different from the residual layer capping on a nocturnal boundary layer, although they are suggested to be the same in Stull's ABL diurnal cycle (Stull, 1988).

Other reanalysis data, such as ERA-40 (Uppala et al., 2005), also provide the ABL depth (by using different parameterizations), but at a larger time interval of 6 hours. By using these 6-hourly data, the calculated residual layer will be too deep and stable. We also calculate the residual layer by using the 3-hourly ERA-interim data (Dee et al., 2011), and find that there is no fundamental difference in its given residual layer compared with 20R for the period of observation in 2012 over Badain Jaran (figure omitted). However, the differences of ABL height in different reanalyses, and their effects on the description of a residual layer should be noted and will be investigated in future work.

3. Results

3.1. *Climatological mean*

Based on the definition in section 2, the climatological mean depth (h_R) and the lapse rate within the residual layer (γ_R) in East Asia are provided in Fig. 3. The maximum h_R is located near the border line between China and Mongolia, over which the maximum h_R is even greater than half of the mean maximum CBL depth (not shown). γ_R exhibits the opposite seasonal variation to h_R. Because the residual layer is more neutral, less energy is consumed when the thermals enter the residual layer (Han et al., 2012), a deeper CBL may be stimulated by a neutral residual layer in summer (Fig. 3c). There are also differences in the climatological mean pattern between h_R and γ_R. The minimum γ_R ($\sim$1.7 K km^{-1}) appears in central west Mongolia in summer, while the deepest residual layer has a more stable stratification at $\sim$3 K km^{-1}. Such a difference is attributed to the effect of the surface sensible heat flux (H_s).

The climatological mean surface sensible heat flux is provided in Fig. 4. The pattern of H_s throughout the year is similar to that of the residual layer depth (and also the CBL depth), which indicates its importance to the climatological mean distribution of the CBL. However, the surface sensible heat flux in summer is concentrated mainly west of 90°E, which is slightly different from the pattern of the residual layer (also for the CBL) depth (Fig. 3c). The neutral residual layer east of 90°E may have enlarged the CBL depth there.

The wind shear within the residual layer (W_{sh}) may also affect the mean pattern of the CBL depth. However, because the climatological mean W_{sh} shows an opposite seasonal variation to that of the CBL depth, its effect may be less important. Similar results were derived from a numerical simulation by Moeng and Sullivan (1994).

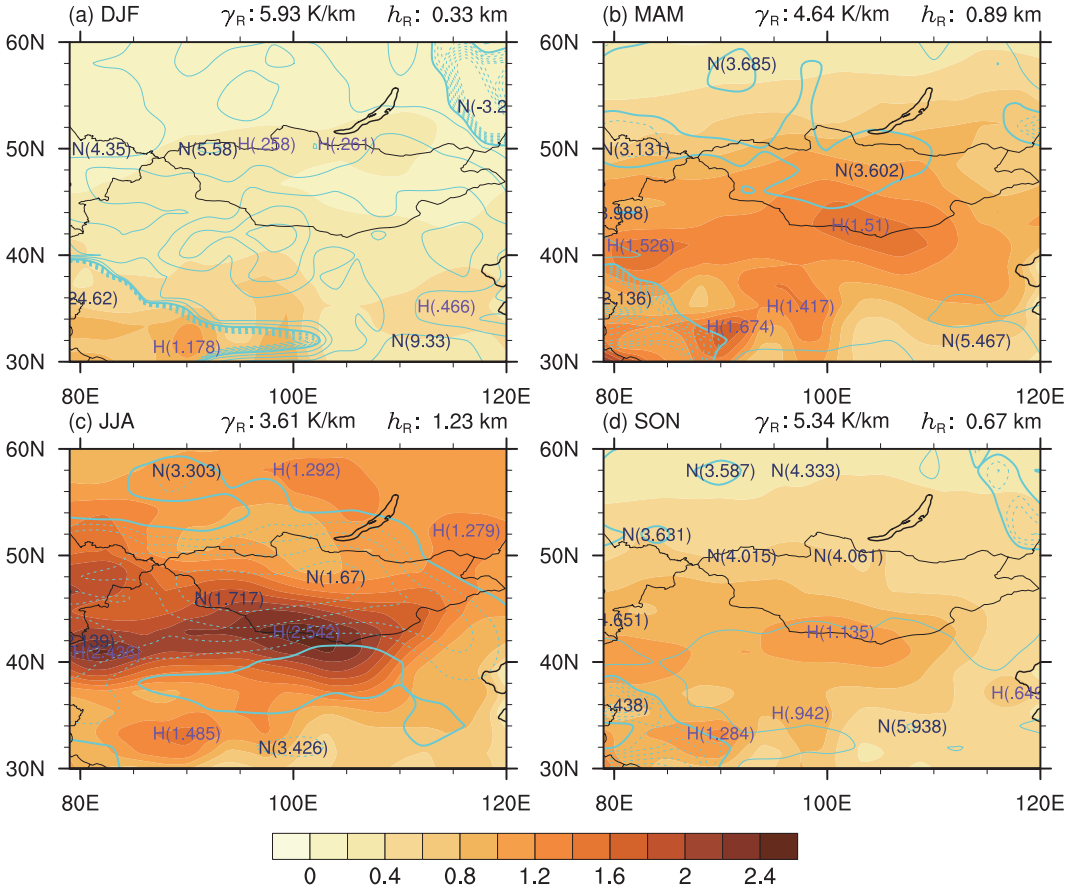

Fig. 3. The climatological mean depth of the residual layer (h_R, color shading, units: 10^3 m) and its lapse rate (γ_R, contours, units: K km^{-1}) in the four seasons from 1970 to 2010. The contour line is dashed for the range of (0, 4) at an interval of 0.5 and solid for the range of (4, $+\infty$) at an interval of 1. The line with a value of 4 is thickened. The regional averaged h_R and γ_R over the entire area is provided at the top of each figure. The location and value for the local maximum h_R (purple H) and the minimum γ_R (blue N) are also indicated in each figure, along with their values in parentheses.

After comparing the climatological means, the potential effects of H_s, W_{sh} and γ_R on the climatological mean CBL depth exhibit significant regional dependence. For example, in the summer, the maximum h_R near (41°N, 82°E) corresponds well with the minimum γ_R; however, the H_s is weaker than its surroundings in that area. At (42°N, 100°E), the much stronger H_s and W_{sh} are likely more responsible for the deep CBL rather than γ_R. Therefore, although the H_s might have dominated the main seasonal variations and patterns of CBL depth, the effects due to residual layer cannot be neglected.

3.2. *Co-variations on an interannual scale*

Compared with the climatological mean patterns, the covariation of variables presents better evidence for their potential connections. In this part of the discussion, the seasonal mean variables will first be calculated; then their regional averages in summer can be obtained. To obtain the seasonal mean depth of the CBL, we first calculate the h_{max} on each day, and then the daily h_{max} can be used to derive the seasonal mean CBL depth in each year. The seasonal mean γ_R and W_{sh} are also obtained following this method.

The linearly regressed anomaly for h_{max} in different seasons at each grid based on the local variations of γ_R is presented in Fig. 5. It is evident that the simultaneous variations of γ_R and h_{max} are the most significant in summer, followed by the spring (MAM), and weakest in the autumn (SON) and winter (DJF). In the summer, γ_R appears to control a large portion of the h_{max} anomaly over the regions between 42°N and 48°N.

Compared with γ_R, the region with significant positive correlation coefficients between h_{max} and W_{sh} is the largest in spring, from the center of Mongolia to the south of Russia (Fig. 6). The maximum h_{max} anomaly regressed by W_{sh} is approximately 127 m. In summer, meanwhile, the regressed h_{max} according to W_{sh} shows a much more complicated structure: Over Mongolia, north of 45°N, the regressed h_{max} is positive, with a maximum value of 181 m; whereas south of 45°N, the regressed h_{max} is negative and the minimum value is −184 m. Although a stronger wind shear seems to be beneficial for the development of the CBL from Eq. (1), large-eddy simulation results given by Han et al. (2012) suggest that it can also suppress the CBL development by sustaining the inversion layer, which may induce the negative correla-

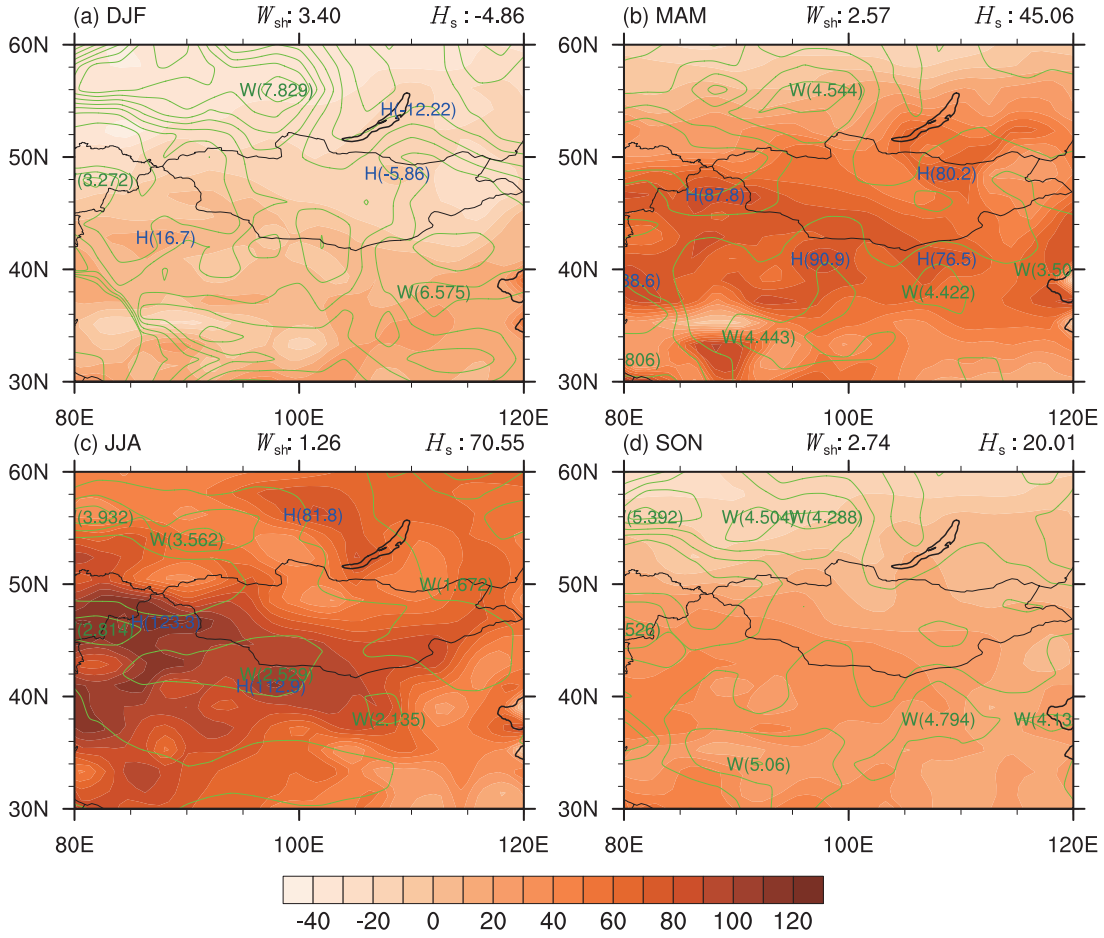

Fig. 4. As in Fig. 3 except for the surface sensible heat flux (H_s, color shading, units: W m^{-2}) and the wind shear within the residual layer (W_{sh}, contour intervals: 10^{-3} s^{-1}). The local maximum H_s (blue H) and maximum W_{sh} (dark green W) are also indicated in each figure, along with their values in parentheses.

tion between W_{sh} and h_{max} to the south of 45°N.

If γ_R and W_{sh} are independent of each other, then their regressed h_{max} anomalies in the summer can be greater than 550 m to the north of 45°N (figure not shown), which is greater than that regressed by the surface sensible heat flux there (Fig. 7). Therefore, the potential contribution of the residual layer to the development of the CBL is comparable to that from surface sensible heat flux over certain locations. To give a clear representation of the relation between the CBL development and other factors that may have influenced it, the regionally averaged summer means of h_{max}, H_s, γ_R and W_{sh} over (40°–50°N, 90°–110°E) from 1970 to 2010 are provided in Fig. 8. All series are normalized to facilitate the comparison. Surprisingly, the correlation coefficient between h_{max} and H_s (0.75) is less significant than that between h_{max} and γ_R (-0.92), although both of them are statistically significant at the 95% confidence level. It is difficult to conclude if the lapse rate of the residual layer is more important for CBL development than that of H_s based on their correlation coefficients alone; however, γ_R seems to be more crucial for h_{max} than H_s at times. For example, in 1972 and 1988, although H_s is stronger in the summer, h_{max} is not deeper, and the stratification of the residual layer is stable; while in 1982 and 1985, even though H_s is not strong, a more neutrally stratified residual layer (presented as a negative normalized γ_R) may have caused a higher h_{max}. The correlation between h_{max} and W_{sh} is poor, which may be caused by the spatial differences in their local correlations (Fig. 5c).

During most periods, a stronger (weaker) H_s and a more neutral (stable) residual layer tends to appear simultaneously in summer. This might be attributed to the fact that a deeper CBL caused by a stronger H_s tends to induce a deeper residual layer. To highlight the independent contribution of the residual layer to the CBL, regardless of H_s, the ratio of the regionally averaged h_{max} and H_s (h_{max}/H_s) and its correlation coefficient with γ_R are given in Fig. 8. γ_R can still explain approximately two-thirds of the residual variation of h_{max} when the contribution from H_s is removed. Therefore, the contribution from a neutrally stratified residual layer may be more important than that from an intense buoyancy flux of a well-developed CBL over the region (40°–50°N, 90°–110°E) in summer.

3.3. *Daily variations*

Because the residual layer is available for every day, it is necessary to check whether the good correspondence be-

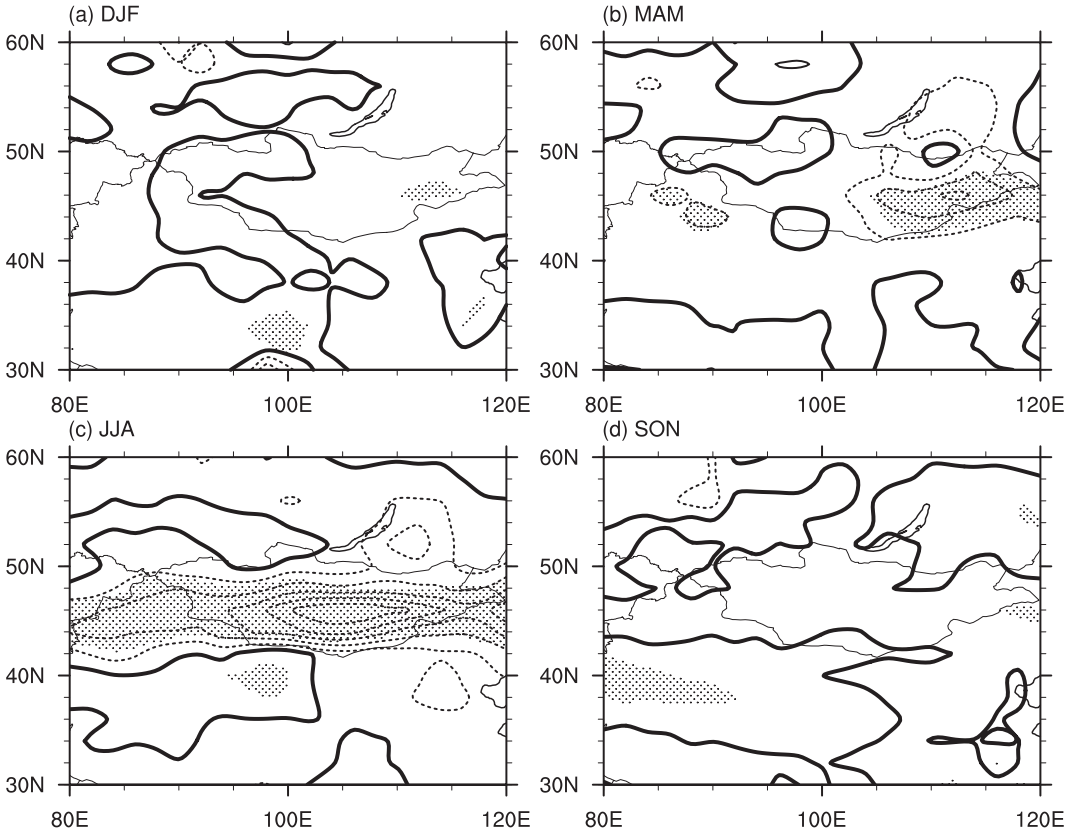

Fig. 5. The linearly regressed anomaly for the annual h_{max} in different seasons according to the local variation of γ_R (contour intervals: 60 m). The 95% confidence levels are stippled. The 0 lines are thickened.

tween the residual layer structure and CBL development can be verified on the daily scale. A field experiment was conducted in the Badain Jaran desert in late August 2009 (Han et al., 2012) and early July 2012 (Fig. 1). Therefore, we first select two periods to investigate the daily variations of the residual layer and CBL. The first period is from 1 August to 31 September 2009, and the second is from 1 June to 31 July 2012. Following previous discussions, the regionally averaged h_{max}, daily maximum H_s (H_{s_max}), γ_R, and W_{sh} over (40°–50°N, 90°–110°E) on each day are presented in Fig. 9; the associated correlation coefficients are listed in Table 2. Because of the significant auto-correlation, the effective number of degrees of freedom [see von Storch and Zwiers (2001) for details] for all of the series is smaller than their sample numbers, which reduces the statistical significance of the correlation coefficients.

Surprisingly, although positive correlation coefficients exist between the original h_{max} and H_{s_max}, their de-trended series have negative correlations in August and September of 2009. The integration of positive H_s during a day (H_{s_day}) exhibits an even more negative correlation with h_{max}. The correlation coefficient between h_{max} and H_{s_max} during June and July in 2012 is positive but insignificant. Therefore, an intense surface sensible heat flux seems to affect the variation of the CBL depth over a long period but not within the daily scale.

The correlation coefficients between γ_R and h_{max} are more statistically significant during both periods. This confirms the importance of the residual layer on CBL development. Furthermore, the one day lead/lag correlation coefficients between γ_R and h_{max} are also significant, at least for the 95% confidence level. This may indicate that a residual layer can retain characteristics of the CBL for two continuous days in this region, which partly confirms the typical diurnal cycle of the ABL given by Stull (1988).

Compared with observations, the development of the regional mean CBL from reanalysis data on 30 and 31 August (Fig. 9) is similar with the observation in Badain Jaran (Han et al., 2012). From the observation experiment, the maximum surface sensible heat flux is about 150 W m^{-2} on 30 August, and the maximum CBL depth is over 3000 m; while on 31 August, although the maximum surface sensible heat flux is approximately 250 W m^{-2}, the maximum CBL depth is just 1800 m. Significant differences occur in the observed lapse rates of the residual layer on these two days. Observed phenomena on these two days is quite similar to the regional averaged results given by 20R. However, the regional averaged maximum CBL depth shows a continuous increase from 3 to 7 July 2012 from 20R, which is not in common with the site observation (Fig. 1). Therefore, even though the representativeness of 20R needs to be further investigated, the relationship among its CBL depth, the lapse rate of the residual layer and the surface sensible heat flux is quite similar as that derived from site observations.

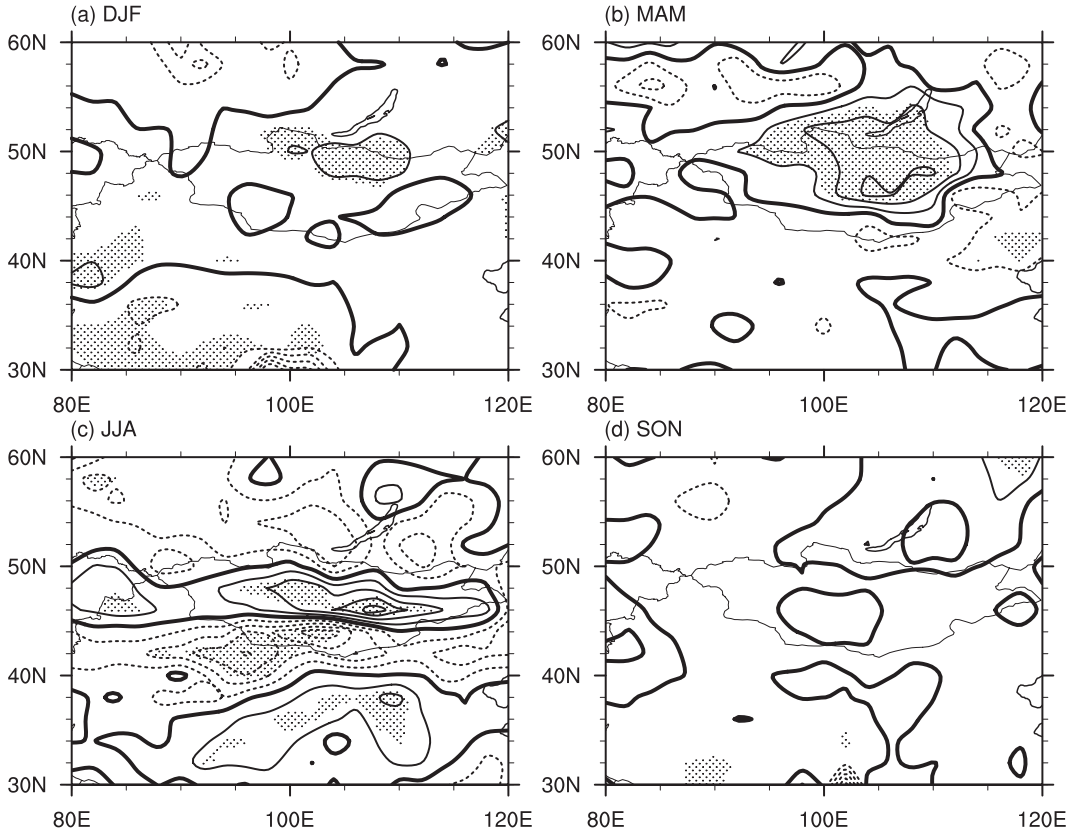

Fig. 6. Similar to Fig. 5 except for the anomaly of h_{max} according to the local variation of the vertical shear of horizontal wind (contour intervals: 40 m).

Table 2. The correlation coefficients of the daily regionally averaged variables with h_{max} from 1 August to 30 September 2009 and from 1 June to 31 July 2012. The results for the original series (O) and de-trended (D) series are listed. The +1 (−1) indicates that the variable listed in the table is leading (lagging) h_{max} by 1 day. The correlation coefficients that are statistically significant at the 95% confidence level are in bold font, and those at the 99% confidence level are in bold-italic font.

		H_{s_max}			H_{s_day}			γ_R			W_{sh}		
		+1	0	−1	+1	0	−1	+1	0	−1	+1	0	−1
2009	O	0.76	0.70	0.65	0.75	0.69	0.65	−0.80	***−0.88***	−0.75	−0.14	−0.07	−0.04
	D	0.09	−0.18	−0.28	−0.00	−0.33	−0.38	**−0.58**	***−0.79***	−0.43	0.20	0.37	0.39
2012	O	0.63	0.60	0.52	0.59	0.54	0.50	**−0.66**	***−0.84***	**−0.72**	0.19	0.38	0.24
	D	0.52	0.45	0.30	0.44	0.33	0.26	−0.55	***−0.80***	**−0.64**	0.27	0.48	0.30

The correlation coefficient between the daily regionally averaged h_{max} and γ_R for each month during 1970–2012 is displayed in Fig. 10a; the results from the de-trended series are displayed in Fig. 10b. The correlation coefficient between h_{max} and γ_R is negative and significant most of the time, especially for the de-trended series. The correlation is the strongest in April and September and weakest in January and July. Considering the seasonal variation of the CBL (Fig. 3), the potential effect of γ_R is strongest when the monthly mean CBL is growing (i.e. April) or decaying (i.e. September). When the monthly mean CBL is at its maximum or minimum, the effect of γ_R becomes much weaker.

The correlation between h_{max} and $H_{s_max}$is nearly opposite to that between h_{max} and γ_R (Figs. 10c and d). Only a few coefficients are statistically significant. Negative values appear more frequently in April and September, although none are statistically significant. The correlations in January and July are larger than those in nearby periods. All of these features infer that the surface sensible heat flux is more influential on CBL development when the residual layer effect is weak.

As per the discussions above, it seems that the effects of H_s and γ_R on the development of the CBL are different. From October to March, when the monthly mean CBL depth is the shallowest in a year (data not shown, but the value can be referred to by the depth of the residual layer in Fig. 3), its daily depth is mainly controlled by H_s. During this period, the residual layer may be too shallow and stably stratified (Fig. 3a) to affect the CBL. From March to May, a nearly neutral residual layer seems to have transmitted the features

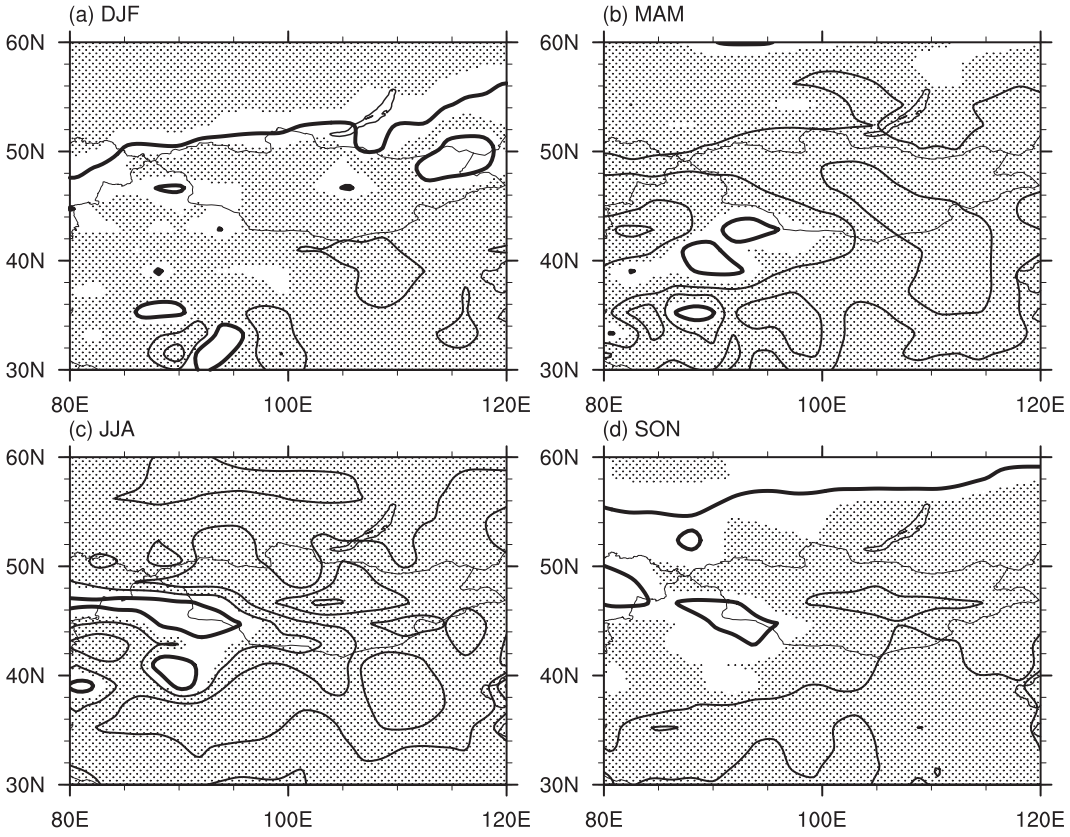

Fig. 7. Similar to Fig. 5 except for the linearly regressed anomaly of h_{max} according to the local variation of sensible heat flux (contour intervals: 100 m).

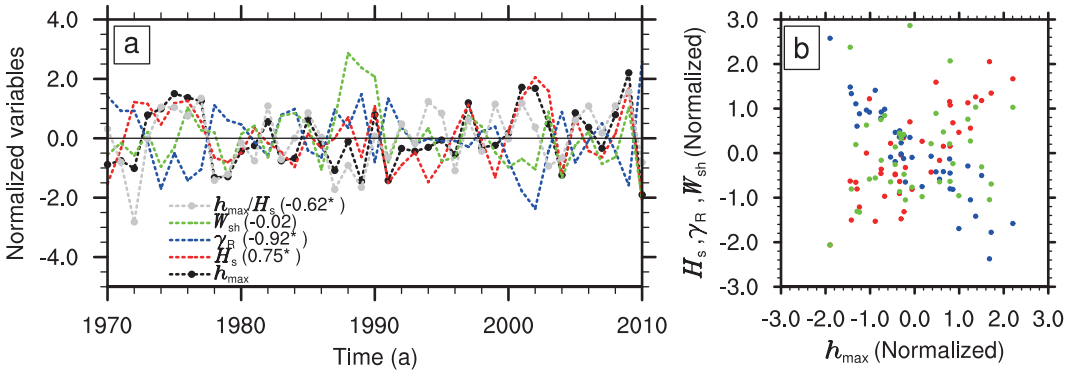

Fig. 8. The time series of normalized summer (JJA) mean h_{max}, H_s, γ_R, W_{sh} and h_{max}/H_s from 1970 to 2012, all of which are averaged over (40°–50°N, 90°–110°E) (a). The correlation coefficients of H_s, γ_R, W_{sh} with h_{max} are provided in parentheses. The correlation coefficient of h_{max}/H_s with γ_R is also provided. A star means the coefficient is statistically significant at the 95% confidence level. The normalized H_s, γ_R and W_{sh} versus h_{max} is given (b). The colors of the scatters are the same as those of the lines in (a).

of the CBL development between days. This is a type of accumulative growth of the CBL: a deep CBL helps maintain a deep and neutral residual layer until another new CBL begins to develop the next morning. Such an effect of the residual layer becomes weak in mid-summer, when the monthly mean CBL depth is close to its maximum in a year. Afterwards, when the monthly mean CBL depth begins to decay, accumulative growth of the CBL becomes significant again. This is evidenced by the fact that the surface sensible heat flux in the autumn is only about two-fifths of that in the spring (Figs. 4b, d), but the CBL depth in autumn is approximately two to three times that in spring. Therefore, the residual layer may have accelerated the increase of the CBL depth in spring, and slowed the decay in autumn.

4. Summary and discussion

This paper analyzes the effect of the residual layer on the CBL development near Mongolia. Based on observations, the depth of the residual layer is subjectively assumed to be

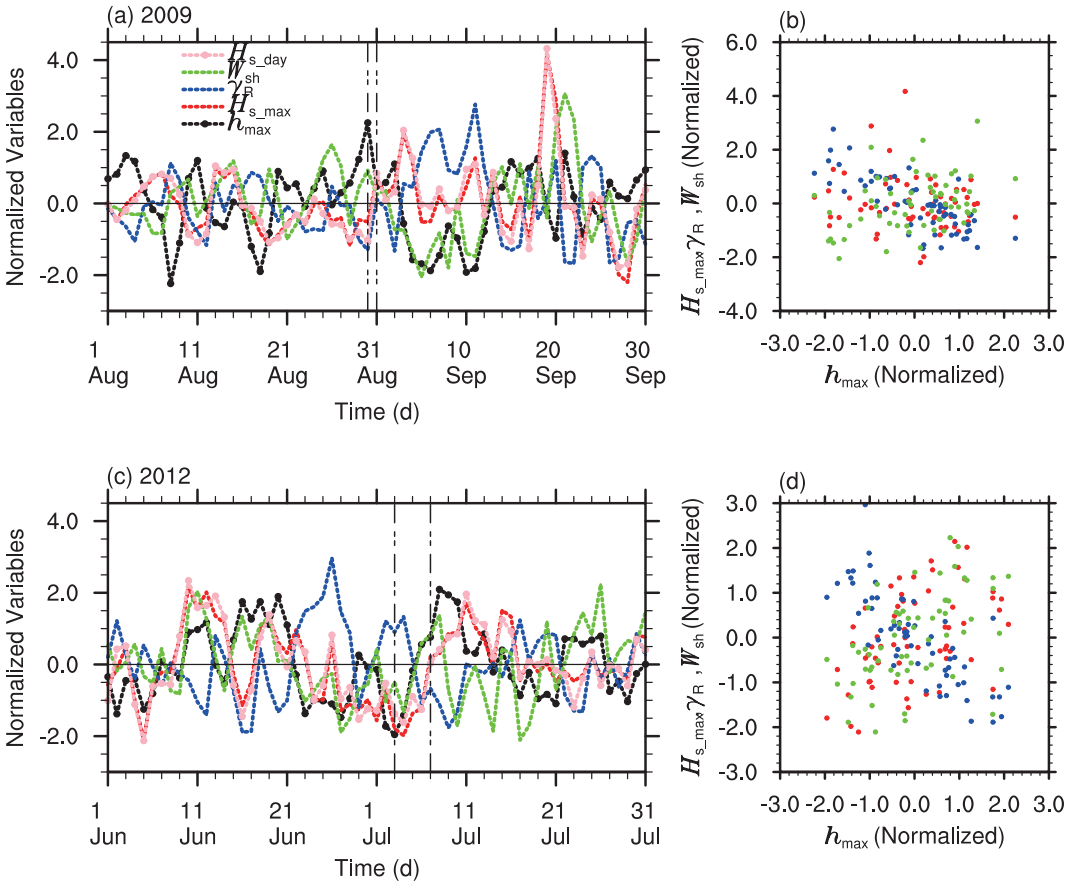

Fig. 9. The daily normalized series of regionally averaged h_{max}, H_{s_max}, γ_R, and W_{sh} over (40°–50°N, 90°–110°E) in (a) 2009 and (c) 2012. The vertical dot-dot-dash lines indicate the period when radiosondes were used in the Badain Jaran observation experiment in 2009 and 2012. The scatter plots for the daily normalized variables versus h_{max} are given in (b) and (d). The color of the scatters is the same as the lines in (a).

equal to the largest growth of the CBL depth in 3 hours. The effect of the residual layer on the development of the CBL is investigated over a large area during 1970–2012. The main conclusions are as follows:

(1) The climatological mean distribution of the CBL depth in each season may be not only determined by the surface sensible heat flux, but also affected by the stratification of the residual layer.

(2) The interannual variations of the seasonal mean CBL depth are significantly correlated with the wind shear and stratification within the residual layer over the region of (40°–50°N, 90°–110°E) in summer. The correlation of the regionally averaged CBL depth with the lapse rate of the residual layer is even stronger than that with the surface sensible heat flux.

(3) On the daily scale, the correlation between the surface sensible heat flux and CBL depth is no longer significant and even becomes negative in April and September. Meanwhile, the lapse rate within the residual layer is still significantly correlated with the CBL depth; thus, the daily variation of the CBL depth may be more influenced by the stratification status within the residual layer than by the buoyancy flux originated from the heating below.

Considering that the definition of the residual layer used in this study assumes a close connection to the growth of the CBL, a discussion of the relationship between the depths of the residual layer and CBL is meaningless. However, if the residual layer is deep enough, then the impact of its stratification from large-scale circulation can be easily observed. Such a process represents the impact of the large-scale circulation on the local CBL development. For example, the contribution of advection and the synoptic-scale circulation on CBL development has been suggested by Bianco et al. (2011); however, the mechanisms responsible have not yet been determined, which may be attributed to the unknown changes in the layer above the CBL. Based on this study, the large-scale circulation can impact the CBL development through changing the structure of the residual layer. Specifically, the study region experiences frequently synoptic activities (Ren et al., 2010). Whether these large-scale processes are connected with the maintenance and variation of the residual layer, and further can affect the local CBL development, requires investigation.

From this study, the correlation between CBL depth and γ_R or W_{sh} over the study region shows significant spatial differences (see Figs. 5 and 6). Such spatial dependency may be caused by the terrain effect. On the continental scale, the

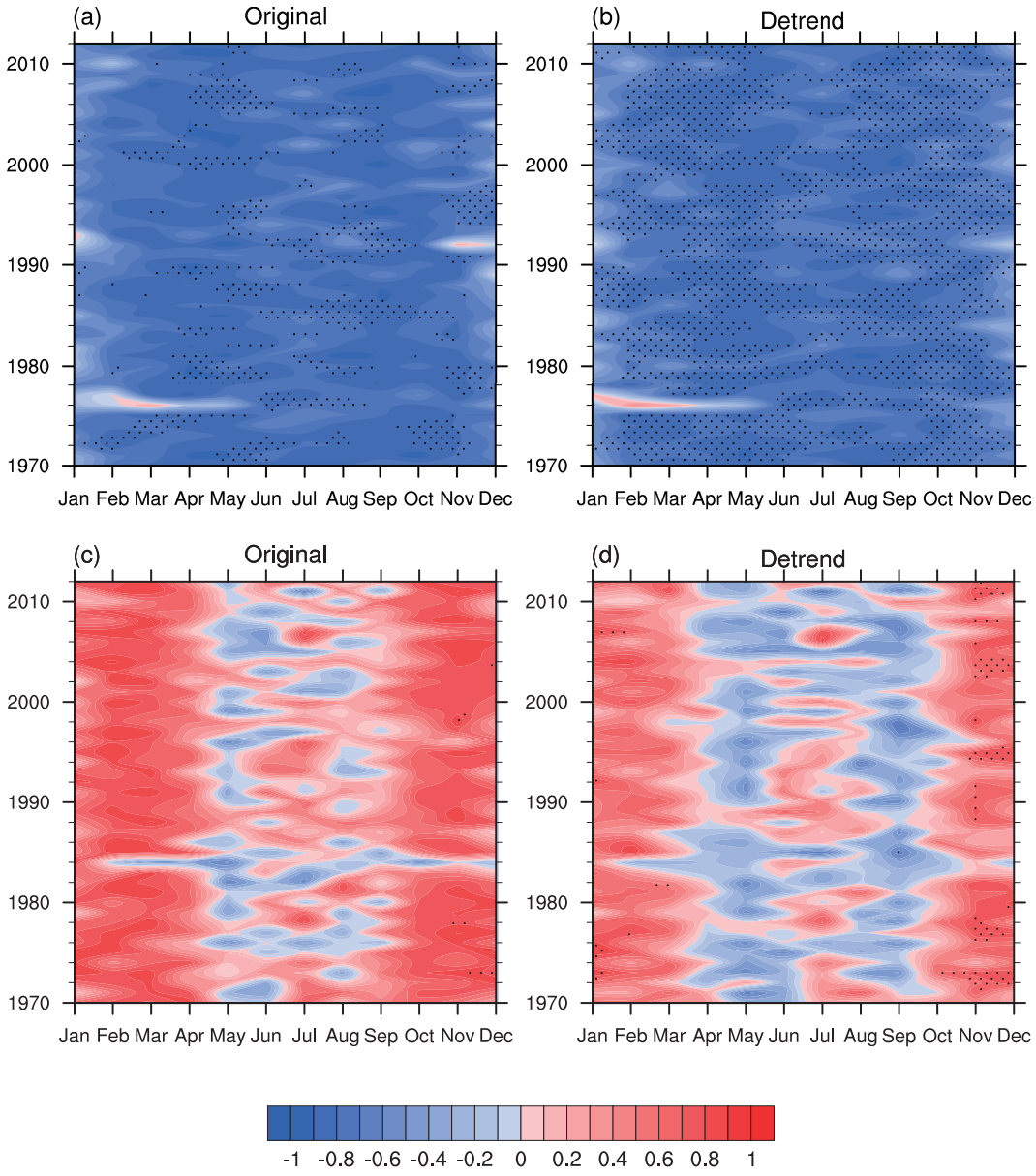

Fig. 10. The daily correlation coefficients between the regionally averaged (40°–50°N, 90°–110°E) h_{max} and γ_R (a, b) and between h_{max} and H_{s_max} (c, d) in every month from 1970 to 2012. The left column is from the original series and the right column is from the de-trended ones. The correlation coefficients that are statistically significant at the 95% confidence level (*t*-test) are dotted.

main circulation over East Asia is modulated by the thermal and dynamic effect of the Tibetan Plateau, which means the thermal structure of the atmosphere at mid-level height will also be impacted. While on a smaller spatial scale, the coupling between the CBL and the slope–valley wind system in mountain regions has been noted for decades (Banta, 1984, 1986; Stensrud, 1993), and the deep residual layer there is quite similar to what we observed in Badain Jaran (Fig. 1).

If the structure above the CBL is mainly impacted by factors such as the large-scale circulation, then the label of "residual layer" should be reconsidered, as its characteristics may no longer be the result or residual of the local CBL development the previous day. This problem has also been identified in the Badain Jaran experiment (Han et al., 2012); the layer above the CBL is called the neutral layer in that study. In this study, the lapse rate of the residual layer is still significantly correlated with the CBL depth on the previous day (Table 2), which indicates that the characteristics of the CBL development can be stored in the residual layer until the following day. Therefore, the capping layer over the CBL can still be considered the residual layer, but its features are not completely determined by the CBL of the previous day.

Acknowledgements. This research was funded by the National Natural Science Foundation of China (Grant No. 41205005), the National Basic Research Program of China (Grant No.

2010CB950503), and the West Light Foundation of the Chinese Academy of Sciences to HAN Bo. The Twentieth Century Reanalysis Project dataset is provided by the U.S. Department of Energy, Office of Science Innovative and Novel Computational Impact on Theory and Experiment (DOE INCITE) program, and Office of Biological and Environmental Research (BER), and by the National Oceanic and Atmospheric Administration Climate Program Office.

REFERENCES

Avissar, R., and T. Schmidt, 1998: An evaluation of the scale at which ground-surface heat flux patchiness affects the convective boundary layer using large-eddy simulations. *J. Atmos. Sci.*, **55**, 2666–2689.

Banta, R. M., 1984: Daytime boundary-layer evolution over mountainous terrain. Part 1. Observations of the dry circulations. *Mon. Wea. Rev.*, **112**, 340–356.

Banta, R. M., 1986: Daytime boundary-layer evolution over mountainous terrain. Part II. Numerical-studies of upslope flow duration. *Mon. Wea. Rev.*, **114**, 1112–1130.

Banta, R. M., and Coauthors, 2011: Dependence of daily peak O-3 concentrations near Houston, Texas on environmental factors: Wind speed, temperature, and boundary-layer depth. *Atmos. Environ.*, **45**, 162–173.

Barthlott, C., J. W. Schipper, N. Kalthoff, B. Adler, C. Kottmeier, A. Blyth, and S. Mobbs, 2010: Model representation of boundary-layer convergence triggering deep convection over complex terrain: A case study from COPS. *Atmospheric Research*, **95**, 172–185.

Bianco, L., I. V. Djalalova, C. W. King, and J. M. Wilczak, 2011: Diurnal evolution and annual variability of boundary-layer height and its correlation to other meteorological variables in California's Central Valley. *Bound.-Layer Meteor.*, **140**, 491–511.

Compo, G. P., and Coauthors, 2011: The twentieth century reanalysis project. *Quart. J. Roy. Meteor. Soc.*, **137**, 1–28.

Dee, D. P., and Coauthors, 2011: The ERA-Interim reanalysis: configuration and performance of the data assimilation system. *Quart. J. Roy. Meteor. Soc.*, **137**, 553–597.

Durre, I., R. S. Vose, and D. B. Wuertz, 2006: Overview of the integrated global radiosonde archive. *J. Climate*, **19**, 53–68.

Elliott, W. P., and D. J. Gaffen, 1991: On the utility of radiosonde humidity archives for climate studies. *Bull. Amer. Meteor. Soc.*, **72**, 1507–1520.

Fedorovich, E., R. Conzemius, and D. Mironov, 2004: Convective entrainment into a shear-free, linearly stratified atmosphere: Bulk models reevaluated through large eddy simulations. *J. Atmos. Sci*, **61**, 281–295.

Fochesatto, G. J., P. Drobinski, C. Flamant, D. Guedalia, C. Sarrat, P. H. Flamant, and J. Pelon, 2001: Evidence of dynamical coupling between the residual layer and the developing convective boundary layer. *Bound.-Layer Meteor.*, **99**, 451–464.

Freire, L. S., and N. L. Dias, 2013: Residual layer effects on the modeling of convective boundary layer growth rates with a slab model using FIFE data. *J. Geophys. Res.*, **118**, 12 869–12 878.

Garratt, J. R., 1994: *The Atmospheric Boundary Layer.* Cambridge University Press, 316 pp.

Gentine, P., A. K. Betts, B. R. Lintner, K. L. Findell, C. C. van Heerwaarden, A. Tzella, and F. D'Andrea, 2013a: A probabilistic bulk model of coupled mixed layer and convection. Part I: Clear-sky case. *J. Atmos. Sci.*, **70**, 1543–1556.

Gentine, P., A. K. Betts, B. R. Lintner, K. L. Findell, C. C. van Heerwaarden, and F. D'Andrea, 2013b: A probabilistic bulk model of coupled mixed layer and convection. Part II: Shallow convection case. *J. Atmos. Sci.*, **70**, 1557–1576.

Han, B., S. H. Lu, and Y. H. Ao, 2012: Development of the convective boundary layer capping with a thick neutral layer in Badanjilin: Observations and simulations. *Adv. Atmos. Sci.*, **29**, 177–192, doi: 10.1007/s00376-011-0207-4.

Holtslag, A. A. M., and B. A. Boville, 1993: Local versus nonlocal boundary-layer diffusion in a global climate model. *J. Climate*, **6**, 1825–1842.

Holtslag, A. A. M., E. I. F. Debruijn, and H. L. Pan, 1990: A high-resolution air-mass transformation model for Short-range weather forecasting. *Mon. Wea. Rev.*, **118**, 1561–1575.

Hong, S. Y., and H. L. Pan, 1996: Nonlocal boundary layer vertical diffusion in a medium-range forecast model. *Mon. Wea. Rev.*, **124**, 2322–2339.

Huang, Q., J. H. Marsham, D. J. Parker, W. S. Tian, and C. M. Grams, 2010: Simulations of the effects of surface heat flux anomalies on stratification, convective growth, and vertical transport within the Saharan boundary layer. *J. Geophys. Res.-Atmos.*, **115**, doi: 10.1029/2009JD012689.

Lenschow, D. H., and P. L. Stephens, 1980: The role of thermals in the convective boundary-layer. *Bound.-Layer Meteor.*, **19**, 509–532.

Lin, J. T., and M. B. McElroy, 2010: Impacts of boundary layer mixing on pollutant vertical profiles in the lower troposphere: Implications to satellite remote sensing. *Atmos. Environ.*, **44**, 1726–1739.

Maronga, B., and S. Raasch, 2013: Large-eddy simulations of surface heterogeneity effects on the convective boundary layer during the LITFASS-2003 experiment. *Bound.-Layer Meteor.*, **146**, 17–44.

Marsham, J. H., D. J. Parker, C. M. Grams, B. T. Johnson, W. M. F. Grey, and A. N. Ross, 2008: Observations of mesoscale and boundary-layer scale circulations affecting dust transport and uplift over the Sahara. *Atmos. Chem. Phys.*, **8**, 6979–6993.

Messager, C., D. J. Parker, O. Reitebuch, A. Agusti-Panareda, C. M. Taylor, and J. Cuesta, 2010: Structure and dynamics of the Saharan atmospheric boundary layer during the West African monsoon onset: Observations and analyses from the research flights of 14 and 17 July 2006. *Quart. J. Roy. Meteor. Soc.*, **136**, 107–124.

Moeng, C. H., and P. P. Sullivan, 1994: A comparison of shear-driven and buoyancy-driven planetary boundary-layer flows. *J. Atmos. Sci.*, **51**, 999–1022.

Pan, H. L., and L. Mahrt, 1987: Interaction between soil hydrology and boundary-layer development. *Bound.-Layer Meteor.*, **38**, 185–202.

Parker, D. J., C. D. Thorncroft, R. R. Burton, and A. Diongue-Niang, 2005: Analysis of the African easterly jet, using aircraft observations from the JET2000 experiment. *Quart. J. Roy. Meteor. Soc.*, **131**, 1461–1482.

Ren, X. J., X. Q. Yang, and C. J. Chu, 2010: Seasonal variations of the synoptic-scale transient eddy activity and polar front jet over East Asia. *J. Climate*, **23**, 3222–3233.

Roy, S. B., and R. Avissar, 2000: Scales of response of the convective boundary layer to land-surface heterogeneity. *Geophys. Res. Lett.*, **27**, 533–536.

Saha, S., and Coauthors, 2010: The NCEP climate forecast system reanalysis. *Bull. Amer. Meteor. Soc.*, **91**, 1015–1057.

Stensrud, D. J., 1993: Elevated residual layers and their influence on surface boundary-layer evolution. *J. Atmos. Sci.*, **50**, 2284–2293.

Stull, R. B., 1976: Mixed-layer depth model based on turbulent energetics. *J. Atmos. Sci.*, **33**, 1268–1278.

Stull, R. B., 1988: *An Introduction to Boundary Layer Meteorology.* Kluwer Academic Publishers, 670 pp.

Tennekes, H., 1973: Model for dynamics of inversion above a convective boundary-layer. *J. Atmos. Sci.*, **30**, 558–567.

Thornton, D. C., A. R. Bandy, and J. G. Hudson, 2011: Fast sulfur dioxide measurements correlated with cloud condensation nuclei spectra in the marine boundary layer. *Atmos. Chem. Phys.*, **11**, 11 511–11 519.

Troen, I., and L. Mahrt, 1986: A simple-model of the atmospheric boundary-layer-sensitivity to surface evaporation. *Bound.-Layer Meteor.*, **37**, 129–148.

Uppala, S. M., and Coauthors, 2005: The ERA-40 re-analysis. *Quart. J. Roy. Meteor. Soc.*, **131**, 2961–3012.

von Storch, H., and F. W. Zwiers, 2001: *Statistical Analysis in Climate Research.* Cambridge University Press, 494 pp.

Zilitinkevich, S., 2012: The height of the atmospheric planetary boundary layer: State of the art and new development. *National Security and Human Health Implications of Climate Change*, H. J. S. Fernando, Z. Klaić, and J. L. McCulley, Eds., Springer Netherlands, 147–161.

Zilitinkevich, S. S., S. A. Tyuryakov, Y. I. Troitskaya, and E. A. Mareev, 2012: Theoretical models of the height of the atmospheric boundary layer and turbulent entrainment at its upper boundary. *Izvestiya, Atmospheric and Oceanic Physics*, **48**, 133–142.